IEEE Access
Multidisciplinary | Rapid Review | Open Access Journal

Received October 18, 2019, accepted October 25, 2019, date of publication October 31, 2019, date of current version November 15, 2019.

Digital Object Identifier 10.1109/ACCESS.2019.2950726

Compact High Gain Resonant Cavity Antenna With via Hole Feed Patch and Hybrid Parasitic Ring Superstrate

DUY-NINH DANG[1] AND CHULHUN SEO[2], (Senior Member, IEEE)
[1]Department of Information Communication, Materials, and Chemistry Convergence Technology, Soongsil University, Seoul 156-743, South Korea
[2]School of Electronic Engineering, Soongsil University, Seoul 156-743, South Korea

Corresponding author: Chulhun Seo (chulhun@ssu.ac.kr)

This work was supported by the National Research Foundation of Korea (NRF) funded by the Korean Government (MSIP) under Grant NRF-2017R1A5A1015596.

ABSTRACT A compact and high gain resonant cavity antenna (RCA) is investigated in this work. At first, a ray-tracing model and the full-wave analysis are presented to clarify the characteristics of RCA in cases of finite lateral size and inhomogeneous superstrate. In consequence, a novel compact, high gain, and wideband RCA is proposed. The RCA consists of a via hole feed patch and an array of hybrid parasitic rings fabricated on a superstrate. The via holes feed patch with a high radiation directivity significantly enhances the RCA's gain. On another hand, the dimension and bandwidth of the RCA are improved by the hybrid parasitic ring superstrate which is constituted by non-periodic parasitic patch and rings. Finally, a prototype of the RCA is fabricated and measured. With only the dimension of $1.35\lambda_0 \times 1.35\lambda_0 \times 0.63\lambda_0$, the peak gain of 15.8 dBi and 3 dB gain bandwidth of 10.7% are obtained.

INDEX TERMS Resonant cavity antenna, compact, high gain, non-periodic microstrip superstrate, hybrid parasitic ring.

I. INTRODUCTION

Compact microwave system with high performance is the trend of future technology, i.e., microwave power transmission, biomedical implant, and 5G handset devices. The increment of operating frequency and the development of manufacturing technology allow the implementation of the compact microwave system. However, the high gain antenna is always a large dimension component in the system because it requests a large radiation area. Designing a compact antenna with high gain and wideband is a big challenge for modern RF and microwave systems [1]–[4].

In recent years, the resonant cavity antenna (RCA), which consists of one or multi-superstrates placing in front of a single or array of feed patches, has been extensively employed due to its high gain. Broadening bandwidth and reducing dimension are also currently works on studying of the RCA [5]–[18]. Relatively, the trade-offs between dimension, gain, and bandwidth are considered in these works. The high gain RCAs are paid by large lateral dimension and narrow bandwidth [5], [13]. In contrast, the compact designs have lower gain than others [7], [12]. Whereas, the compact RCAs obtaining high gain and wideband require multi-superstrate layers [6], [15], [16], [18] or complex superstrate structures [8], [10], [14], [17]. These RCAs have been focused on the study of novel feed patch and superstrate structures.

The feed patch is not only the excited source but also decides the performance of RCA. The radiation efficiency, bandwidth, and directivity of RCA are commonly proportional to those of the feed patch. Several popular techniques enhancing the performance of the feed patch are air-substrate, array of patches, and reactive impedance surface. The structure of a metallic patch on low-cost air-substrate expresses low dielectric loss and high radiation efficiency. But it is not a robust structure and hard fabrication in the manufacture, especially for small antenna [5], [12], [14]. Meanwhile the array of patches is a good technique to enhance directivity; however, its drawbacks are the large area and requirement of a complex feeding network [9], [12]. Otherwise, the reactive impedance surface acts as a perfect reflecting electric or magnetic surfaces. The reactive impedance surface decreases the interaction between the feed patch and its substrate, which

The associate editor coordinating the review of this manuscript and approving it for publication was Yang Yang.

TABLE 1. Charateristics of three general structures of periodic microstrip superstrate.

Type of MSs	Behavior	Objective index	Element width	Element spacing
MM slab	Effective homogeneous medium	Negative permeability/permittivity	$<\lambda/4$	Adjacent
FSS	Lattice dispersion	High reflectivity	$\sim \lambda/2$	Adjacent
PPs	Resonant structure	180^o out of phase of E-field at FP and parasitics	$\sim \lambda/2$	$\sim \lambda/2$

results in suppressing of surface waves and improving in impedance matching and antenna efficiency [9], [12], [15]. The disadvantage of the reactive impedance surface is a complex structure with numerous cells that raises the design period and cost of antenna. In this work, a single microstrip patch with loading of via holes is proposed as the feed patch of the RCA. The via hole feed patch achieves high gain and narrow beamwidth as well as easy to fabrication.

On another hand, the superstrate structures were dominantly investigated in the literature. The RCA superstrates are popularly classified into two types, homogeneous dielectric superstrate (HDS) [7], [11] and microstrip superstrate (MS) [5], [6], [8]–[10], [12]–[18]. In [7], the same reflection coefficients and effects on the performance of the RCA with homogeneous dielectric and microstrip superstrates were proved by the mathematical and numerical methods. However, the accuracy of such work is restricted by conditions of substrates' dimensions and materials. Recently, the RCAs with microstrip superstrate are attractive structures with various configurations. Three general microstrip superstrates are frequency selective surface (FSS) [6], [10], [12]–[14], [17], metamaterial slab (MM slab) [10], [15], [16], [18], and parasitic patches (PPs) [5], [9], [14]. Their brief behaviors are summarized in Table 1. These structures are almost periodic microstrip superstrates which are arrayed from an original element called a cell. Otherwise, a non-periodic microstrip superstrate is a printed circuit board with different metal elements. Because the fields that propagate from the feed patch to each metal element have different path lengths and phases, the non-periodic microstrip superstrate is applied to control the phase of the metal elements to get in-phase between them. Therefore, the RCA with non-periodic microstrip superstrate is more efficient than the periodic structure [19]–[22]. In the same lateral dimension, the non-periodic parasitic patch superstrate is more suitable than the others because it requires a much less number of elements. Based on the non-periodic parasitic patch superstrate, this work proposes a novel hybrid parasitic ring superstrate, which is constituted by non-periodic parasitic patch and rings. The hybrid parasitic ring superstrate is proved as a compact and high gain structure. Furthermore, its dual-band characteristic is utilized to broaden the bandwidth of the RCA.

The rest of the paper is organized as follows. The ray-tracing model of RCA in cases of finite reflecting surfaces and inhomogeneous superstrate is proposed in section II. In addition, the full-wave analysis is presented to clarify the characteristic of RCA further. Consequently, section III describes the novel RCA with the via hole feed patch and the hybrid parasitic ring superstrate. In section IV, a prototype of this RCA is fabricated and measured. Finally, the conclusion is made in Section V.

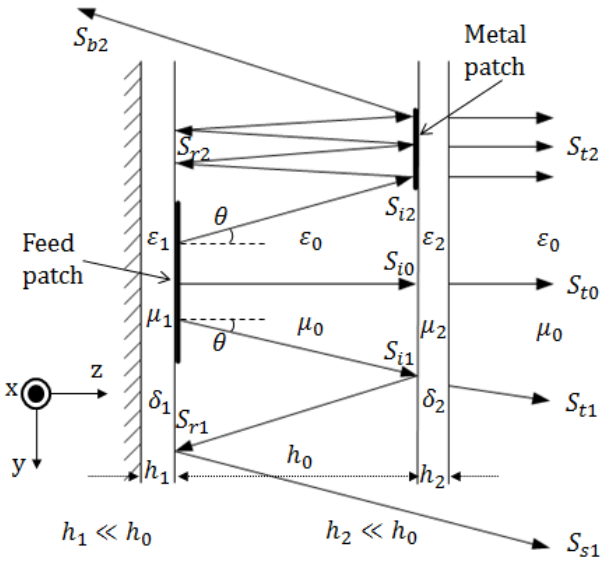

FIGURE 1. Ray-tracing model of RCA with finite reflecting surfaces and a thin superstrate.

II. RCA WITH FINITE REFLECTING SURFACES

The first model of RCA was proposed by Trentini with an infinite perfect reflecting ground and a partially reflecting superstrate [23]. The superstrate is modeled as a surface without the contribution of its thickness and dielectric constant. On the other hand, the homogeneous medium of superstrate (with thickness h, relative permittivity ϵ, relative permeability β) is cautiously examined in [7]. In these works, the reflection and transmission equations are summed up from infinite numbers of reflected and transmitted waves. In fact, the dimension of RCA is finite, which limits the number of reflected and transmitted waves. Furthermore, the microstrip superstrate is a complex dielectric-metal textured material which is different from the conventional dielectric superstrate. Therefore, an RCA model with finite reflecting surfaces and inhomogeneous superstrate should be considered.

A. RCA'S RAY-TRACING MODEL

The ray-tracing model of RCA with finite reflecting surfaces is proposed in Fig. 1. The feed patch and conducting ground are fabricated separately on two faces of a homogeneous substrate (h_1, ϵ_1, β_1, and dielectric loss μ_1). The superstrate

TABLE 2. RCAs with various feed patchs and superstrates.

No.	Feed patch(FP)	Superstrate
1	Conventional microstrip	-
2	Four PIN microstrip	-
3	Conventional microstrip	HDS ($h_2 = \lambda_2/16$)
4	Conventional microstrip	HDS ($h_2 = \lambda_2/4$)
5	Conventional microstrip	Periodic PPs ($h_2 = \lambda_2/16$)
6	Four PIN microstrip patch	Periodic PPs ($h_2 = \lambda_2/16$)

is comparatively divided into two-part, microstrip and homogeneous dielectric (h_2, ϵ_2, β_2, and μ_2). The air-gap (h_0, ϵ_0, β_0) between feed patch and superstrate possesses thickness about integer of half a wavelength $\lambda_0/2$ to the satisfy resonant condition. The operation of RCA is estimated through the trace of three incident rays S_{i0}, S_{i1}, and S_{i2}. S_{i0} is normal to superstrate surface (incident angle $\theta = 0$), only leaks out of the cavity without any reflection to the ground plane. The transmitted part S_{t0} totally contributes to the directivity of RCA. The oblique ray S_{i1} to the dielectric part ($\theta > 0$) partially reflects a ray S_{r1} to ground plane and leaks ray S_{t1} out of the cavity. Since the superstrate's dielectric constant is larger than the air-gap, and the transmitted angle of S_{t1} is smaller than θ, the dielectric superstrate tends to focus on incident rays from the feed patch. Because of the finite reflecting surfaces, the reflection of S_{r1} on the ground plane S_{s1} leaks out of the cavity with reflected angle θ that might widen the RCA's beamwidth; even if, it causes an increment of the RCA's sidelobe level in case of large θ. Another oblique ray S_{i2} to part of microstrip element ($\theta > 0$) obtains multi-reflection with the reflected angle smaller than θ due to the resonant effect of metal patch. Consequently, the multi-transmission rays are generated with a much smaller transmitted angle than θ that is equivalent to the strong convergence to the directivity of the transmitted rays. However, the number of reflections is also limited by the finite reflecting surfaces with the last backward ray of S_{b2} that significantly contributes to the far-field radiation pattern of the back lobe or side lobe.

The above model presents the fundamental difference between finite and infinite RCAs' models that is the number of reflections inside the cavity. Therefore, the reflection and transmission coefficients' equations, which are summed up by mathematical method, are incorrect in the case of finite RCAs and complex dielectric-metal textured materials. Furthermore, in previous works [7], [23], the mathematical equations derived under the condition of the lossless medium are not precise for real materials of feed patch substrate and superstrate. In consequence, the full-wave solution is proper for the compact RCAs. The full-wave simulation is employed to visually express the electromagnetic field and calculate the coefficients of RCAs.

B. FULL-WAVE ANALYSIS

This work studies six antennas with different configurations of feed patch and superstrate, as listed in Table 2. Two kinds of feed patches are conventional and shorting PIN microstrip patches. The feed patches are etched on a high-frequency laminate substrate of Taconic TLY ($\epsilon_1 =\sim 2.2$, $h_1 = 1.2mm$). This substrate offers excellent electrical performance and improves yields of high-frequency laminates for boards requiring tightly controlled impedances. Besides, it is also well characterized in terms of circuit fabrication processing, including for drilling, plating, circuit etching, and finishing [24]. To enhance gain and remain simple structure of the microstrip feed patch, the technique of loading a few shorting PINs is the proper selection. The inductive effect of shorting pin tunes up the resonant frequency, which leads to an increase in the radiation area. Hence, its radiation directivity is enhanced [25], [26]. The superstrates also include two types, homogeneous dielectric and microstrip, with the same material of low cost and high dielectric constant ($\epsilon_2 =\sim 4.4$, $h_2 = 1.52mm$) FR4 substrate. The dielectric superstrate is studied with different thicknesses of superstrate, while the microstrip structure is 3×3 periodic parasitic patches with an array area of $1.25\lambda_0 \times 1.25\lambda_0$.

Figure 2 illustrates Poynting vectors of 6 antennas with the same lateral size of $2\lambda_0 \times 2\lambda_0$. The corresponding reflection coefficients versus operating frequency and realized gains versus lateral sizes of these antennas are plotted in Fig. 3. All of these antennas resonate at 5.8 GHz with a narrow bandwidth (about 2%). Antenna 1 is a square conventional microstrip patch with the patch's approximate width of half a substrate wavelength $\lambda_1/2$. The narrow radiation area of the conventional patch causes a broad divergence of radiation rays that reduce radiation directivity. The radiation area is doubly enlarged in antenna 2 with four PINs loaded inside the boundary of the patch, as presented in [25]. Thus, the divergence of radiation rays notably decreases. The realized gain of antenna 2 is enhanced by about 3 dB in comparison with antenna 1, as shown in Fig. 3(b). Then, the FR4 superstrates with thicknesses of $\lambda_2/16$ and $\lambda_2/4$ are respectively placed above the conventional feed patch in case of antennas 3 and 4. While antenna 4 expresses the strong reflection as well as focusing diverged ray from feed patch, antenna 3 only quite concentrates radiation ray. Therefore, compared to antenna 1, the maximum gain enhancement of antenna 3 is about 3 dB, while the enhancement of antenna 4 is up to 6 dB. However, the high profile and weight of antenna 4 is the main reason preventing it from many applications.

The high gain RCA with a thin superstrate can be achieved by using a periodic microstrip superstrate as presented by antenna 5 and antenna 6. This superstrate comprises the periodic parasitic patches etched below the surface of the FR4 superstrate. This combination creates a complex dielectric-metal textured material that increases the reflection coefficient of superstrate [27]. On another view, each parasitic patch can play a role of radiation element excited by the feed patch. The width and inter-spacing of parasitic elements are $\lambda_2/2$, which satisfies the self-resonant condition. Similar to the antenna array, the radiation directivity of the RCA enhances when the number of the parasitic elements increases. To verify the contribution of the feed patch on the

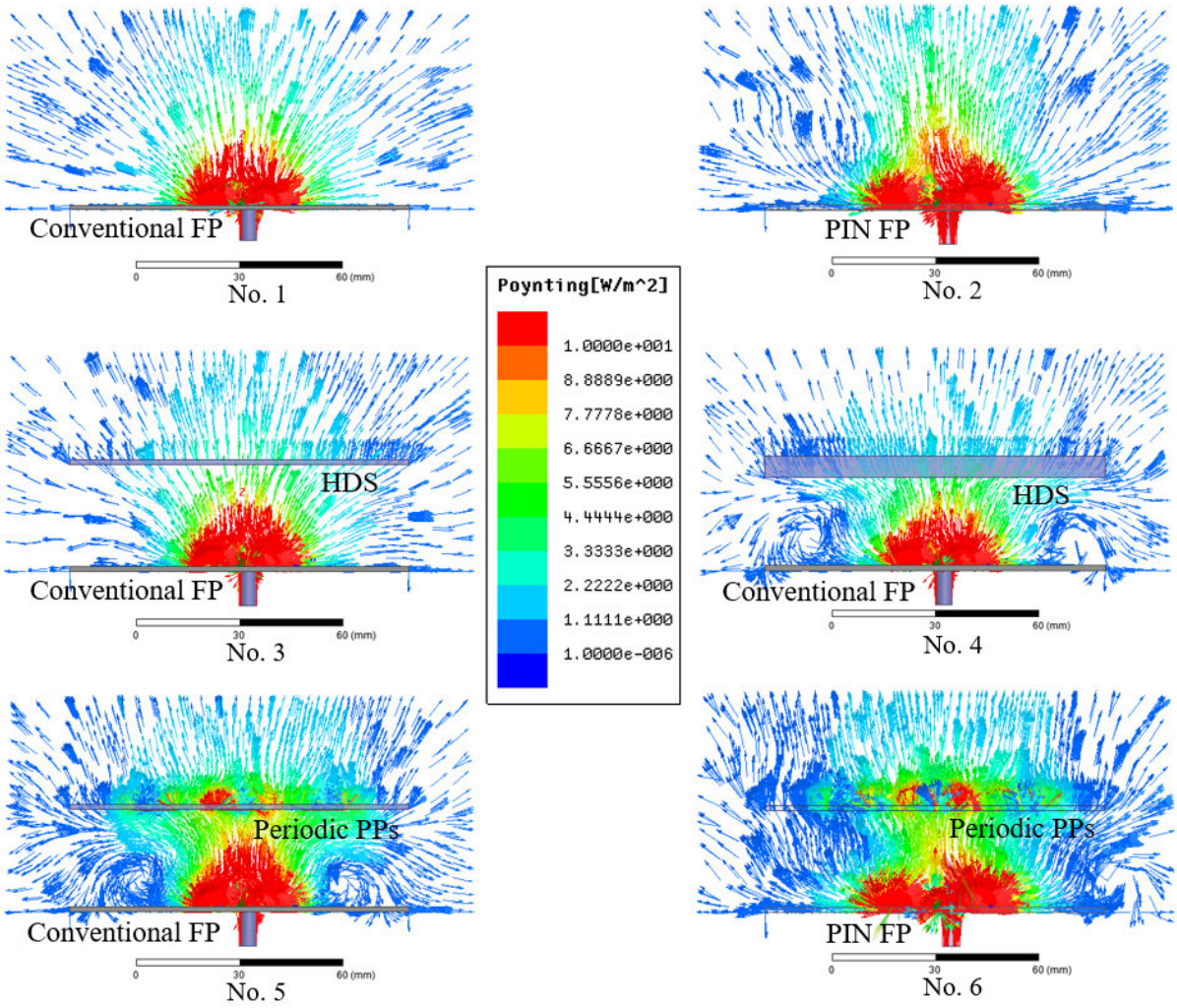

FIGURE 2. Poynting vectors of 6 antennas with the same lateral size of $2\lambda_0 \times 2\lambda_0$.

RCA, the comparing gain enhancements of antenna 5 and antenna 6 to that of antenna 1 is examined. The gain enhancement of antenna 5 with the conventional feed patch is about 7 dB. The highest gain enhancement of 8 dB is presented by antenna 6 with the four shorting PIN feed patch, which provides high directivity and narrow beamwidth feed patch (small incident angle θ).

The dependence of RCA performance on the lateral size of the reflecting surfaces is presented in Fig. 3(b). For a lossless medium, the radiation directivity is proportional to the area of reflecting surfaces. Practically, the dielectric loss of the superstrate is proportional to its volume. The increase in lateral size leads to an increase in the reflection and the dielectric loss of the superstrate. Far from the feed patch, the amplitude of reflection gradually decreases while the dielectric loss is linearly increased with lateral size. Thus, the realized gain of RCA is only optimal at the unique lateral size of reflecting surfaces. Especially for antenna 4, the thick superstrate generates much loss, significantly reducing radiation with a large area. This figure also indicates the efficiency of high directivity feed patch in case of compact reflecting surfaces; however, this advantage diminishes with the increment of superstrate size, as plotted by results of antennas 5 and 6. When the superstrate size is enough to cover wide beamwidth of the conventional feed patch, the reflection and focus of antenna 5 will approach to the antenna 6.

Based on the ray-tracing model and the full-wave simulations, the characteristic of RCA in the case of finite size is clarified. The high directivity feed patch and the high resonant microstrip superstrate are keys to access the high gain, low profile, and compact RCA. This work recognizes the role of microstrip superstrate as radiation planes of RCA with the feed patch as the excited source. Different from antenna array with uniform current source divided by feeding network, the excitation from the feed patch to each microstrip element is non-uniform with various incident angles and amplitude tapering. The periodic microstrip superstrate imperfectly controls these incident waves to correct phase relationship

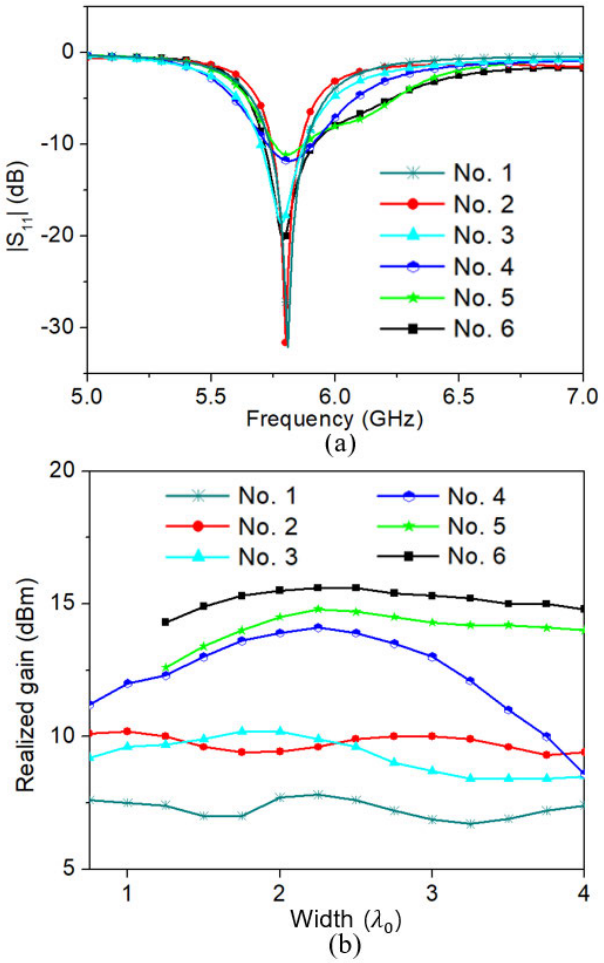

FIGURE 3. Antennas' parameters: (a) Reflection coefficient. (b) Realized gain.

to enhance the power radiated in desired directions. Another shortcoming of periodic microstrip structure is single resonance causing narrow bandwidth. To solve these issues, a novel structure will be proposed in the next section.

III. PROPOSED RCA WITH VIA HOLES AND HYBRID PARASITIC RINGS

A novel wideband, high gain, and compact RCA is proposed as illustrated in Fig. 4. This antenna includes via hole feed patch and hybrid parasitic ring superstrate as a non-periodic microstrip superstrate. The via hole feed patch possesses high directivity and narrow beamwidth. The non-periodic microstrip superstrate controls radiation waves in phase and broads bandwidth by generating two adjacent resonant frequencies. The compact RCA dues to the novel hybrid parasitic ring superstrate constituted by non-periodic square parasitic rings and patch. The design procedure of the proposed non-periodic microstrip superstrate is illustrated in Fig. 5.

A. HIGH DIRECTIVITY FEED PATCH

With the same shunt inductive effect, the shorting pins are replaced by via holes to neglect the soldering step

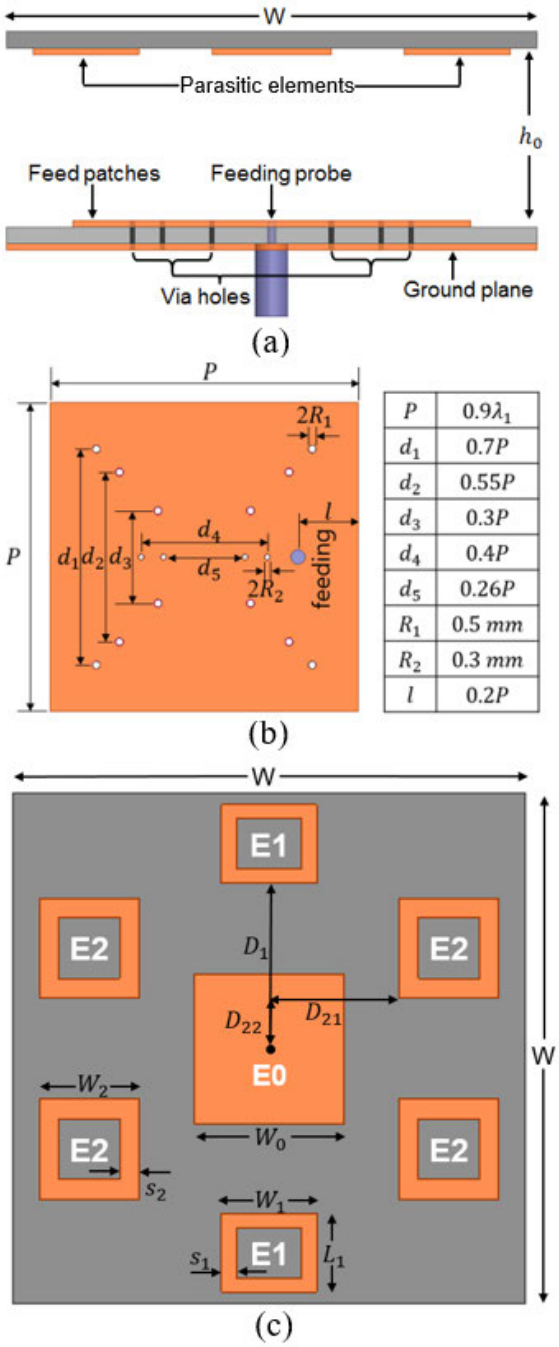

FIGURE 4. Proposed RCA: (a) Side view. (b) Via hole feed patch. (c) Hybrid parasitic ring superstrate.

and reduce the tolerance between simulated and measured results [28]. Figure 4(b) illustrates a feed patch fabricated with 16 via holes on the Taconic TLY substrate with a thickness of 1.2 mm. The reason for selecting the thickness of 1.2 mm is explained in Fig. 6(a) that plots the width and the realized gain of feed patch versus the thickness of the substrate. In the case of the conventional patch, the thickness substrate is proportional to the realized gain and inversely proportional to the patch size. Similarly, the width of via hole patch is also inversely proportional to the thickness of the

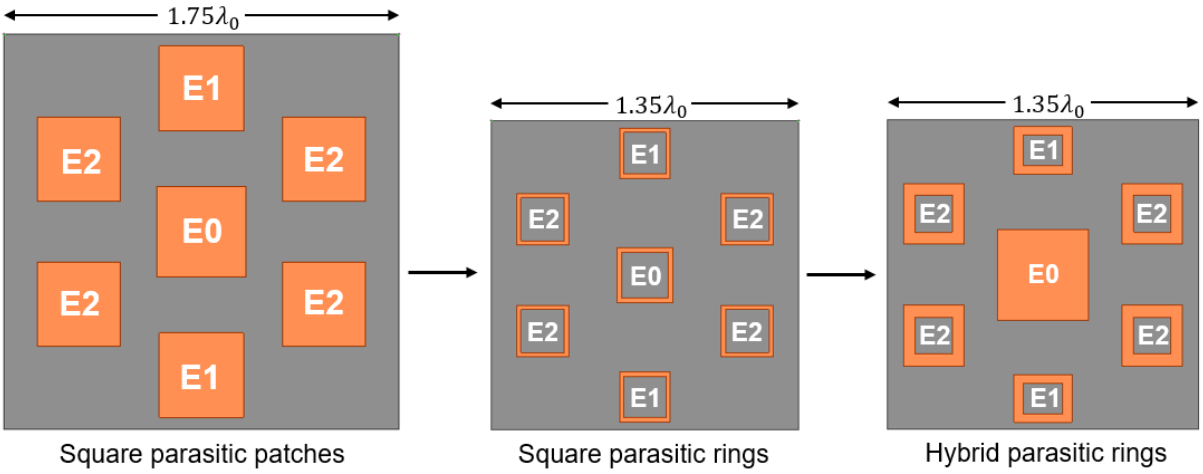

FIGURE 5. Design procedure of the hybrid parasitic ring superstrate.

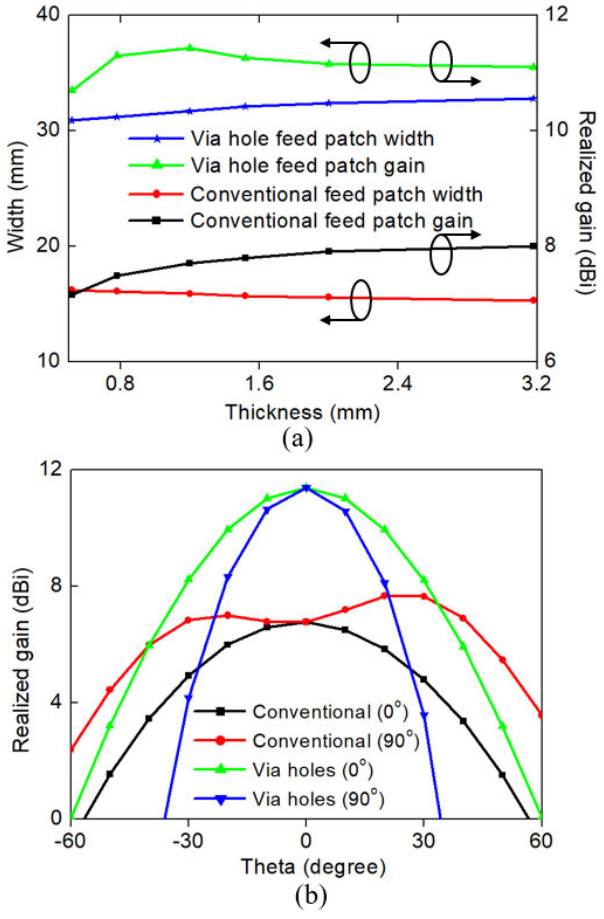

FIGURE 6. Conventional and via hole feed patch parameters: (a) Realized gain and width versus thickness of substrate. (b) Realized gain with $\phi = 0°, 90°$.

substrate; however, the highest realized gain is only achieved at the optimal thickness of the substrate. This point is significantly valuable in designing a compact and low profile antenna.

Due to the inductive effect of via holes, the width of the feed patch is enlarged to $0.9\lambda_1$ comparing to $0.5\lambda_1$ of the conventional one. The realized gains of conventional and via hole feed patch in two principal planes ($\phi = 0°$ and $\phi = 90°$) are compared, as shown in Fig. 6(b). Due to shunt inductive of the via holes, the feed patch has a peak gain of 11.5 dBi corresponding to gain enhancement of 4.6 dB. The via hole patch also has a notably narrow radiation beam compared to the conventional one. In addition, the high radiation efficiency of the via hole feed patch is 96%. As a result, the via hole feed patch is a good candidate to enhance the performance of the RCA.

B. COMPACT NON-PERIODIC MICROSTRIP SUPERSTRATE

As shown in Fig. 5, an array of seven square parasitic patches are firstly arrayed on the bottom side of the FR4 superstrate with a thickness of 1.52 mm. The configuration of these patches is based on the E-field distribution on the bottom surface of the homogeneous dielectric superstrate plotted in Fig. 7. In the case of the via hole feed patch, the E-field is distributed at different levels descending from the center of the dielectric superstrate. Each level is a contour line with an almost elliptical ring shape. As a consequence, these elements are arranged as six elements lying on an elliptical ring around a center patch. These elements are divided into three groups, including E0, E1, and E2. Their dimension and inter-element spacing are determined to satisfy the resonant condition, which is expressed by the 180° out of phase between the electric fields at the parasitic patches and the feed patch. For via holes one, the electric field on the surface of the feed patch is nonhomogeneous, which causes the shunt inductive effect of via holes. The square parasitic patches are installed with the direction of currents on their surfaces as opposed to the direction of dominant currents on the surface of via hole feed patch, as plotted in Fig. 8.

The array area of square parasitic patch superstrate is $1.75\lambda_0 \times 1.75\lambda_0$ with the peak gain of 16.5 dBi at 5.8 GHz in comparison with $2\lambda_0 \times 2\lambda_0$ and 15.8 dBi in Gupta's work [22]. The improvement of the current work is mainly due to the enhancement of directivity and a narrow beamwidth of the via hole feed patch. In another comparison with periodic

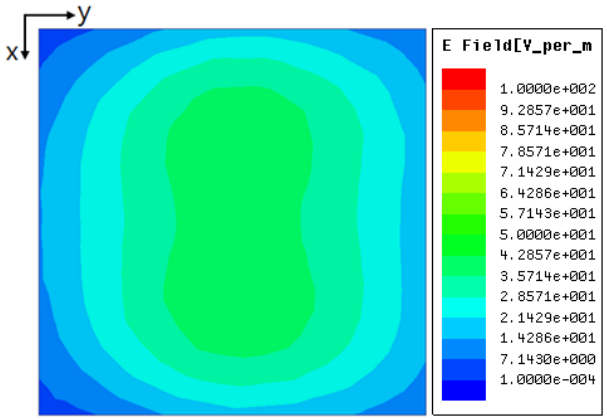

FIGURE 7. E-field distribution on surface of homogeneous dielectric superstrate.

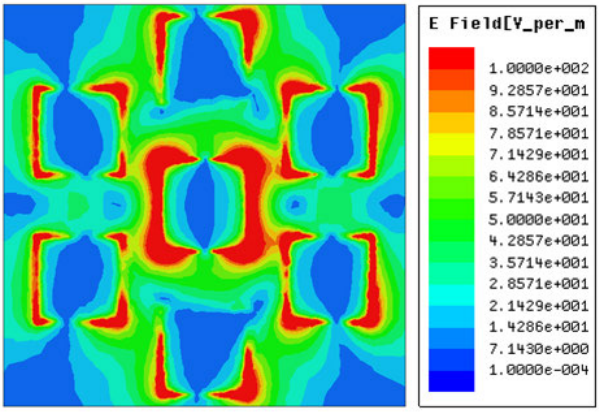

FIGURE 9. E-field distribution on surface of square parasitic patch superstrate.

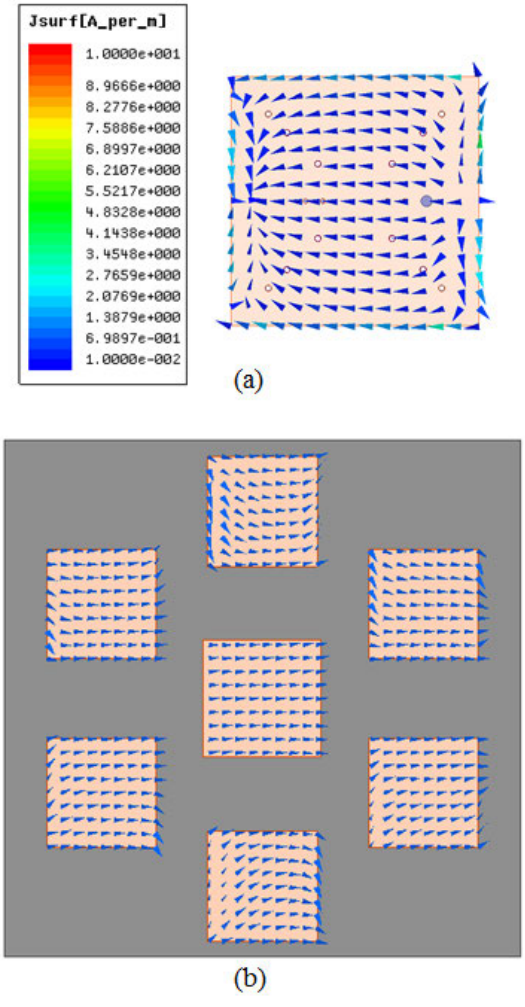

FIGURE 8. Current distributions on square parasitic patch RCA's surfaces: (a) On feed patch surface. (b) On surfaces of parasitic elements.

parasitic patches in the previous section, the gain enhancement is up to 2.2 dB by the reasonable arrangement of parasitic elements. The high resonance is approached by incorporating the self-resonance of each parasitic element and the mutual coupling between them. The inter-coupling increases when the spacing between elements decreases that orders the increment of the element's width to guarantee the self-resonance. Therefore, the lateral size of the non-periodic square parasitic patch superstrate is much larger than the periodic one.

From the perspective of radiation elements, the resonance can be represented by a smaller structure; the simplest one is square ring [29]. The alternative ability of ring structure is proved by analyzing the E-field distribution on the surface of the superstrate where parasitic elements are etched, as illustrated in Fig. 9. The E-field dominantly concentrates on the edge of the patches region and gradually reduces to the inside region. On the central region, the E-field almost shows no distribution. The square parasitic ring is proposed by removing the non-contributed region. For simplicity, this work firstly investigates the single square parasitic ring through the relation between the width of parasitic patch W_0 and its edge s_0, as shown in Fig. 10. In case of a single square parasitic patch with a width of $\lambda_2/2$ (12.7mm), the RCA has a realized gain of 13 dBi. The same results are also achieved by using the parasitic ring with proper selections of W_0 and s_0. Figure 10(b) plots the dimensions of the parasitic ring that has the same performance as the single parasitic patch. The width of the ring reduces when the width of its edge also reduces. In this work, the smallest value of s_0 is 0.2mm that is local capacity for fabrication. The highest value of s_0 requires W_0 to have the same value in case of the single patch. As a consequence, the seven square parasitic rings with the smallest s_0 shown in Fig. 6, presents a compact superstrate with array lateral size of $1.35\lambda_0 \times 1.35\lambda_0$. The widths of elements are significantly reduced while their positions are almost unchanged, which increases the spacing between them. Figure 11(b) shows the E-field distribution on the surface of the parasitic ring superstrate. The strong self-resonances are still obtained with the small rings; however, the inter-couplings decrease, leading to reductions in directivity and gain.

To compensate the inter-coupling, the hybrid parasitic ring structure is proposed. The E0 element is a patch because its size does not affect the dimension of the superstrate. Whereas,

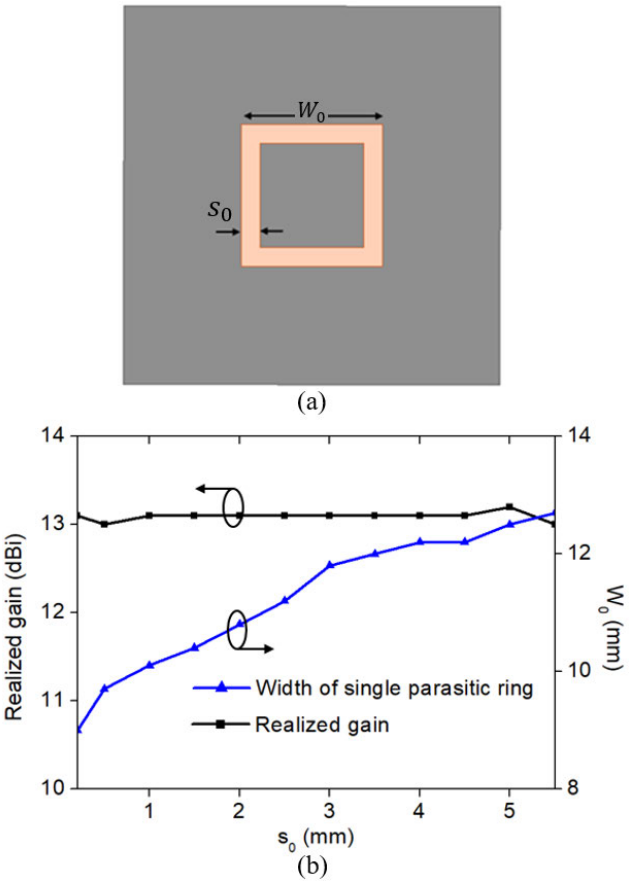

FIGURE 10. Single square parasitic ring: (a) Configuration. (b) Realized gain and W_0 versus s_0.

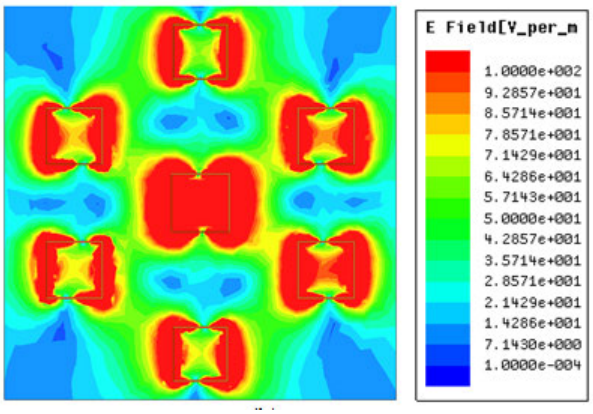

FIGURE 11. E-field distribution on surface of square parasitic ring superstrate.

the E1 and E2 elements are parasitic rings with proper widths selected to reduce the spacing between these elements. Especially, E1 is converted from square to rectangular shape to optimize the vertical dimension of the superstrate but still ensure the resonant condition. Thus, the array size of the optimized superstrate is equal to the square parasitic ring. Delicately, the hybrid structure is compact, as well as providing high resonances. The dimensions of three non-periodic

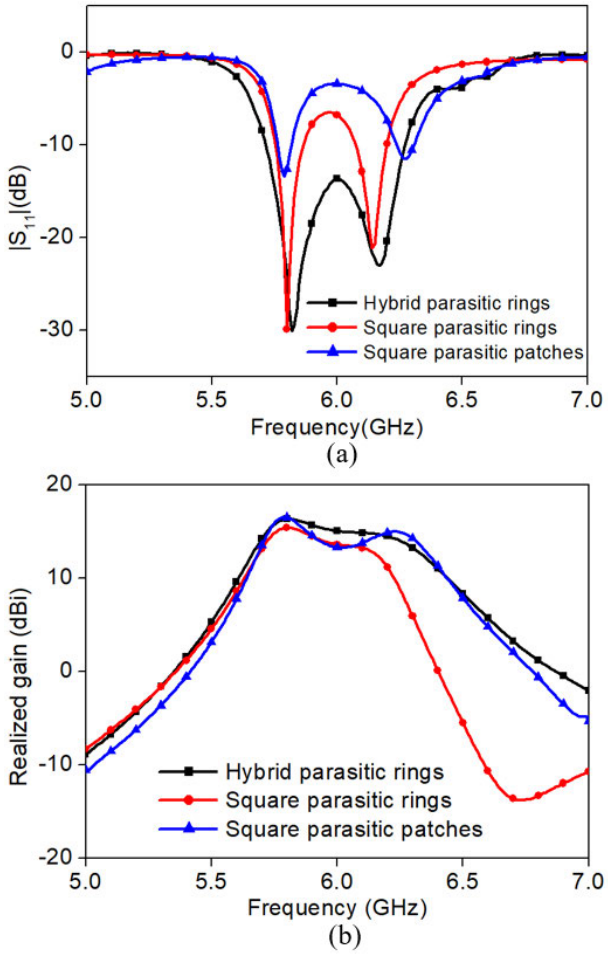

FIGURE 12. RCAs characteristics versus frequencies: (a) Reflection coefficient. (b) Realized gain.

microstrip superstrates are listed in Table 3. The characteristics of corresponding RCAs are plotted in Fig. 12. The peak gains of the square parasitic patches (SPPs), square parasitic rings (SPRs), and hybrid parasitic rings (HPRs) are 15.4 dBi, 16.5 dBi, and 16.3 dBi, respectively. The lateral sizes of these RCAs are $1.35\lambda_0 \times 1.35\lambda_0$, $1.70\lambda_0 \times 1.70\lambda_0$, and $1.35\lambda_0 \times 1.35\lambda_0$. The high gain and compact features are obtained, especially for the hybrid parasitic ring structure.

In terms of bandwidth (BW), the 3 dB gain BWs of the square parasitic patch, square parasitic ring, and hybrid parasitic ring RCAs are 4.7%, 8.3%, and 10.7%, respectively. These results are a huge extension in comparison with the periodic parasitic patches with only approximate 2%. The key point of this extension is dual-resonances generated by the non-periodic structure, as shown in Fig. 12(a). The different lengths of parasitic elements possess different self-resonant frequencies. The contribution of each resonance to the operating frequency of RCA relies on its distance to the feed patch. Meanwhile, the arrangement of many adjacent resonances can extend the bandwidth. To simply control the resonances, the element's order is defined as a set of elements having the same distance (in the circular array) or relatively same distance (as ellipse array) to the feed patch. For this

TABLE 3. Parasitic elemets's dimensions and inter-spacing of 3 superstrates.

Type of MSs	E0		E1			E2					Array size
	$W_0(\lambda_2)$	$s_0(mm)$	$W_1(\lambda_2)$	$L_1(\lambda_2)$	$s_1(mm)$	$D_1(\lambda_2)$	$W_2(\lambda_2)$	$s_2(mm)$	$D_{21}(\lambda_2)$	$D_{22}(\lambda_2)$	$\lambda_0 \times \lambda_0$
SPPs	0.81	-	0.76	0.76	-	0.91	0.75	-	0.73	0.28	1.75×1.75
SPRs	0.42	0.2	0.39	0.39	0.2	0.87	0.40	-	0.69	0.27	1.35×1.35
HPRs	0.81	-	0.52	0.43	2	0.9	0.54	4	0.7	0.28	1.35×1.35

work, seven elements can be divided into two orders. The first order is E0, and the second one includes E1 and E2, which have approximate widths and distances to the feed patch. The dominant resonance at 5.8 GHz is decided by the first one. Another resonance at a higher frequency is due to the second order. The gap between resonances depends on the difference in length between the orders. In the case of square parasitic patches, dual-resonances are not adjacent to each other, so this RCA operates as a dual-band antenna rather than the wideband antenna. In the case of square parasitic ring superstrate, the different dimension of the first and second orders is smaller than other cases; therefore, the square ring superstrate's second resonant frequency is smaller than other cases. Whereas, the hybrid parasitic ring RCA has a wider bandwidth than other cases because its second resonant frequency is high and adjacent to the first resonance. To further expand the bandwidth, the increase in the number of resonances is required, and so is the addition of the parasitic element's order.

IV. RESULTS AND DISCUSSION

To validate the proposed structure, the prototype of RCA with the hybrid parasitic ring superstrate is fabricated, as shown in Fig. 13. The overall dimension of this antenna is $1.35\lambda_0 \times 1.35\lambda_0 \times 0.63\lambda_0$. The height of RCA includes the thickness of the feed patch substrate h_1, thickness of the superstrate h_2, and the distance between them h_0 which is around $0.5\lambda_0$ to satisfy the resonant condition of RCA. In the implementation, the optimal h_0 is $0.578\lambda_0$ for achieving high gain and wideband. The reflection coefficient S_{11} is measured using the HP 8719D vector network analyzer with covering frequencies from 50 MHz to 13.5 GHz. The radiation characteristics of the prototype are measured in the microwave anechoic chamber. The prototype is placed in the far-field of the transmitting antenna and mounted on a positioned that can be rotated freely, as shown in Fig. 14. To measure the radiation pattern of RCA as a function of angle, the prototype is rotated so that the transmitting antenna illuminates the prototype from different angles.

The simulated and measured reflection coefficient and realized gain versus frequencies are shown in Fig. 15. The dual resonant frequencies in the simulation are 5.8 GHz and 6.2 GHz, whereas the measured results are 5.77 GHz and 6.23 GHz. Besides, the magnitude of the reflection coefficient increases in measurement. The measured -10 dB S_{11} bandwidth is 9.6%, while the simulated result is 10.7%. The tolerance between simulation and measurement is caused by dielectric loss, soldering, and fabrication error. Similarly,

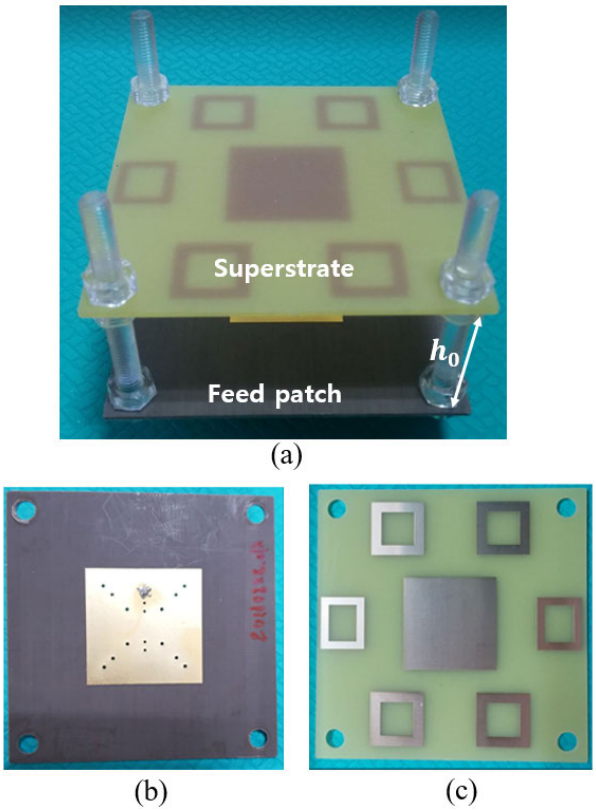

FIGURE 13. Prototype of proposed RCA: (a) Side view. (b) Via hole feed patch. (c) Hybrid parasitic ring superstrate.

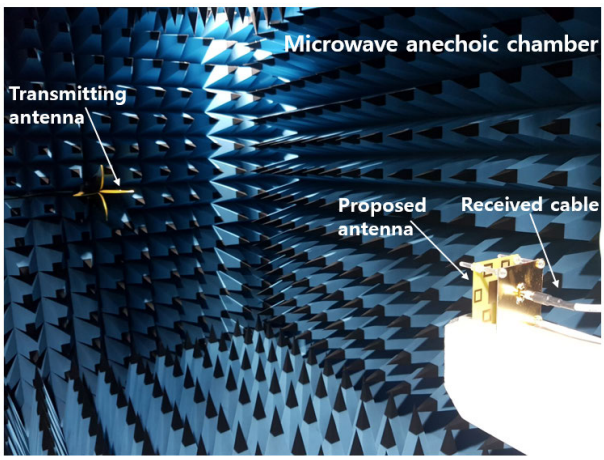

FIGURE 14. Radiation pattern measurement setup.

the measured realized gain also slightly reduces; however, the 3 dB gain bandwidth is still wide as simulated results of 10.7 %. The peak gain is 15.8 dBi at 5.8 GHz with the

TABLE 4. Comparison with a few recently proposed PRSs.

Year/Ref.	Dimension	RCA parameters			PRS parameters		
	$\lambda_0 \times \lambda_0 \times \lambda_0$	Peak gain (dBi)	BW(%)	Aperture Eff. (%)	Type of PRS	Number of layer	Number of unit cells
2014 [5]	$5.00 \times 5.00 \times 0.50$	17.30	2.60	90.0	PPs	1	81
2015 [6]	$3.65 \times 3.65 \times 0.75$	16.30	10.9	N/A	FSS	3	300
2015 [7]	$1.93 \times 1.93 \times 0.63$	13.80	15.9	N/A	HDS	1	0
2016 [8]	$2.50 \times 2.50 \times 0.63$	15.00	10.0	90.0	FSS	1	49
2016 [9]	$2.50 \times 2.50 \times 0.50$	15.80	11.1	70.0	PPs	1	4
2017 [10]	$2.21 \times 2.21 \times 0.58$	16.35	9.36	92.4	MM slab	1	25
2018 [11]	$2.75 \times 2.75 \times 0.56$	16.00	23.0	41.9	HDS	1	0
2018 [12]	$1.55 \times 1.55 \times 0.11$	12.50	24.3	53.7	FSS	1	169
2018 [13]	$3.00 \times 3.00 \times 0.67$	17.78	9.00	90.0	FSS	1	49
2018 [14]	$2.83 \times 3.23 \times 0.49$	17.40	11.6	N/A	PPs + FSS	1	13PPs + 504FSS
2018 [15]	$1.54 \times 1.54 \times 0.83$	14.50	14.0	96.0	MM slab	2	120
2018 [16]	$3.36 \times 3.36 \times 0.70$	19.20	44.4	58.6	MM slab	2	128
2019 [17]	$1.95 \times 1.95 \times 0.58$	15.75	21.5	83.0	FSS	1	99
2019 [18]	$1.80 \times 1.80 \times 0.56$	15.49	10.8	97.5	MM slab	3	48
This work	$1.35 \times 1.35 \times 0.63$	15.80	10.7	95.0	PPs	1	7

PRS: Partially Reflecting Surface λ_0: air wavelength BW: 3dB gain Bandwidth N/A: Not available PPs: Parasitic Patches.
FSS: Frequency Selective Surface HDS: Homogeneous Dielectric Superstrate MM slab: Metamaterial slab.

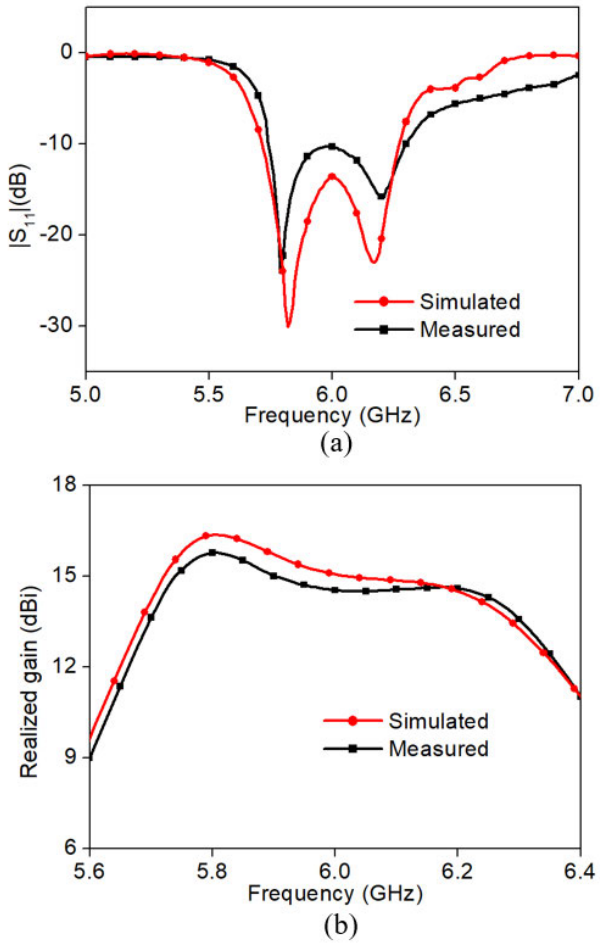

FIGURE 15. Simulated and measured results of proposed RCA: (a) Reflection coefficient. (b) Realized gain.

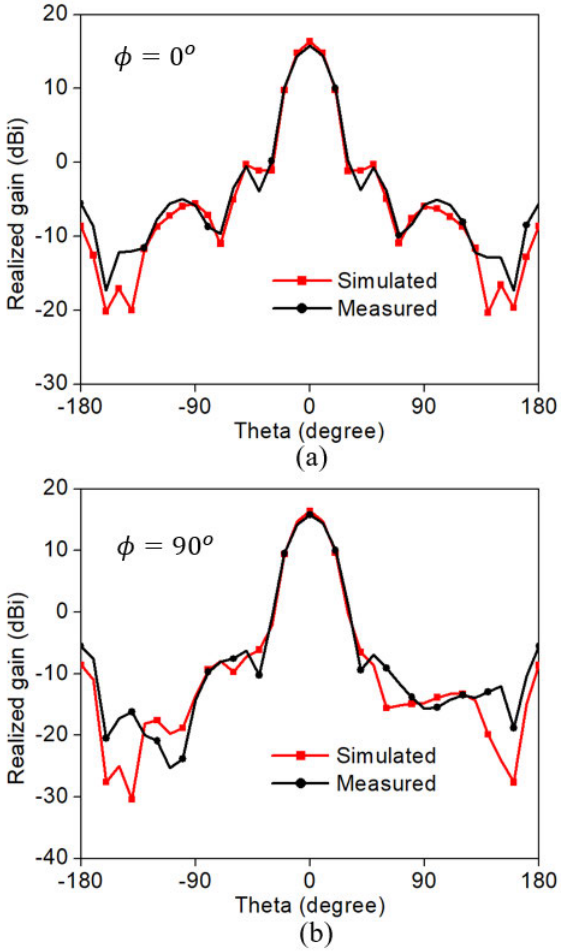

FIGURE 16. Realized gain of proposed RCA in two principal plane at 5.8 GHz: (a) $\phi = 0°$. (b) $\phi = 90°$.

co-polarization radiation pattern in two principal planes ($\phi = 0°$ and $\phi = 90°$) plotted in Fig. 16. The front to back ratio is more than 20 dB in both planes. The sidelobe levels are -16.4 dB and -22.7 dB in $\phi = 0°$ and $\phi = 90°$ planes, respectively. The aperture efficiency is 95%. As summarized in Table 4, the proposed design is compared to several current

published works, highlighting the improved performance of the proposed RCA.

The results indicate that a good agreement between the simulation and measurement is achieved. The tolerance between simulation and measurement mainly comes from the variation of low-cost FR4 substrate's characteristics at high-frequency [20]. At high frequency, the dielectric loss increases while the dielectric constant decreases. There are some works which concentrated on studying FR4 characteristics at high-frequency [30], [31]. However, these works only used the microstrip line model to analyze FR4's characteristics, which is unlike to 3D structure of the antenna. The investigation of the characteristics of FR4 for superstrate in RCA is out of the scope of this work.

V. CONCLUSION

In this work, the combination of the ray-tracing model and the full-wave solution illumines the characteristics of RCA in the case of finite reflecting surfaces. The high directivity feed patch and the non-periodic microstrip superstrate are demonstrated to be effective in the high gain and compact RCA design. In consequence, the RCA with via hole feed patch and hybrid parasitic ring superstrate is proposed. The via holes feed patch provides high gain and narrow beamwidth features as well as the advantage in fabrication. The proposed hybrid parasitic ring superstrate presents a compact, high resonance, and wideband structure. A prototype of the proposed RCA was fabricated with the overall dimension of $1.35\lambda_0 \times 1.35\lambda_0 \times 0.63\lambda_0$, the peak gain of 15.8 dBi, and 3 dB gain BW of 10.7%. The efficiency of this work is proved by comparing with current articles.

REFERENCES

[1] C. R. Valenta and G. D. Durgin, "Harvesting wireless power: Survey of energy-harvester conversion efficiency in far-field, wireless power transfer systems," *IEEE Microw. Mag.*, vol. 15, no. 4, pp. 108–120, Jun. 2014.

[2] O. Galinina, H. Tabassum, K. Mikhaylov, S. Andreev, E. Hossain, and Y. Koucheryavy, "On feasibility of 5G-grade dedicated RF charging technology for wireless-powered wearables," *IEEE Wireless Commun.*, vol. 23, no. 2, pp. 28–37, Apr. 2016.

[3] C. Garcia-Pardo, C. Andreu, A. Fornes-Leal, S. Castelló-Palacios, S. Perez-Simbor, M. Barbi, A. Vallés-Lluch, and N. Cardona, "Ultrawideband technology for medical in-body sensor networks: An overview of the human body as a propagation medium, phantoms, and approaches for propagation analysis," *IEEE Antennas Propag. Mag.*, vol. 60, no. 3, pp. 19–33, Jun. 2018.

[4] M. K. Hedayati, A. Abdipour, R. S. Shirazi, M. J. Ammann, M. John, C. Cetintepe, and R. B. Staszewski, "Challenges in on-chip antenna design and integration with RF receiver front-end circuitry in nanoscale CMOS for 5G communication systems," *IEEE Access*, vol. 7, pp. 43190–43204, 2019.

[5] A. R. Vaidya, R. K. Gupta, S. K. Mishra, and J. Mukherjee, "Right-hand/left-hand circularly polarized high-gain antennas using partially reflective surfaces," *IEEE Antennas Wireless Propag. Lett.*, vol. 13, pp. 431–434, 2014.

[6] K. Konstantinidis, A. P. Feresidis, and P. S. Hall, "Broadband subwavelength profile high-gain antennas based on multi-layer metasurfaces," *IEEE Trans. Antennas Propag.*, vol. 63, no. 1, pp. 423–427, Jan. 2015.

[7] X. Chen, Z. Luo, Z. Zheng, P. Feng, and K. Huang, "Effective reflective characteristics of superstrates and their effects on the resonant cavity antenna," *IEEE Trans. Antennas Propag.*, vol. 63, no. 4, pp. 1572–1580, Apr. 2015.

[8] M. Akbari, S. Gupta, M. Farahani, A. R. Sebak, and T. A. Denidni, "Gain enhancement of circularly polarized dielectric resonator antenna based on FSS superstrate for MMW applications," *IEEE Trans. Antennas Propag.*, vol. 64, no. 12, pp. 5542–5546, Dec. 2016.

[9] S. Dalvi, S. Jagtap, V. Yadav, and R. K. Gupta, "High gain wideband 2×2 microstrip array antenna using RIS and Fabry Perot Cavity resonator," in *Proc. Int. Conf. Microelectron., Comput. Commun. (MicroCom)*, Durgapur, India, Jan. 2016, pp. 1–6.

[10] A. K. Singh, M. P. Abegaonkar, and S. K. Koul, "High-gain and high-aperture-efficiency cavity resonator antenna using metamaterial superstrate," *IEEE Antennas Wireless Propag. Lett.*, vol. 16, pp. 2388–2391, 2017.

[11] L.-Y. Ji, P.-Y. Qin, and Y. J. Guo, "Wideband Fabry–Pérot cavity antenna with a shaped ground plane," *IEEE Accesss*, vol. 6, pp. 2291–2297, 2017.

[12] S. Jagtap, A. Chaudhari, N. Chaskar, S. Kharche, and R. K. Gupta, "A wideband microstrip array design using RIS and PRS layers," *IEEE Antennas Wireless Propag. Lett.*, vol. 17, no. 3, pp. 509–512, Mar. 2018.

[13] M. Asaadi, I. Afifi, and A.-R. Sebak, "High gain and wideband high dense dielectric patch antenna using FSS superstrate for millimeter-wave applications," *IEEE Access*, vol. 6, pp. 38243–38250, 2018.

[14] S. D. Jagtap, R. K. Gupta, N. Chaskar, S. U. Kharche, and R. Thakare, "Gain and bandwidth enhancement of circularly polarized MSA using PRS and AMC layers," *Prog. Electromagn. Res. C*, vol. 87, pp. 107–118, 2018.

[15] B. Majumder, K. Kandasamy, and K. P. Ray, "A zero index based metalens loaded wideband directive antenna combined with reactive impedance surface," *IEEE Access*, vol. 6, pp. 28746–28754, 2018.

[16] Y. Jia, Y. Liu, W. Zhang, J. Wang, S. Gong, and G. Liao, "High-gain Fabry–Pérot antennas with wideband low monostatic RCS using phase gradient metasurface," *IEEE Access*, vol. 7, pp. 4816–4824, 2018.

[17] A. Lalbakhsh, M. U. Afzal, K. P. Esselle, S. L. Smith, and B. A. Zeb, "Single-dielectric wideband partially reflecting surface with variable reflection components for realization of a compact high-gain resonant cavity antenna," *IEEE Trans Antennas Propag.*, vol. 67, no. 3, pp. 1916–1921, Mar. 2019.

[18] A. K. Singh, M. P. Abegaonkar, and S. K. Koul, "Compact near zero index metasurface lens with high aperture efficiency for antenna radiation characteristic enhancement," *IET Microw., Antennas Propag.*, vol. 13, no. 8, pp. 1248–1254, Jun. 2019.

[19] Z. Liu, W. Zhang, D. Fu, Y. Gu, and Z. Ge, "Broadband Fabry–Pérot resonator printed antennas using FSS superstrate with dissimilar size," *Microw. Opt. Technol. Lett.*, vol. 50, no. 6, pp. 1623–1627, Jun. 2008.

[20] R. K. Gupta and J. Mukherjee, "Low cost efficient high gain antenna using array of parasitic patches on a superstrate layer," *Microw. Opt. Technol. Lett.*, vol. 51, no. 3, pp. 733–739, Mar. 2009.

[21] L. Zhou, X. Chen, and X. Duan, "Fabry–Pérot resonator antenna with high aperture efficiency using a double-layer nonuniform superstrate," *IEEE Trans. Antennas Propag.*, vol. 66, no. 4, pp. 2061–2066, Apr. 2018.

[22] R. K. Gupta and J. Mukherjee, "Efficient high gain with low sidelobe level antenna structures using circular array of square parasitic patches on a superstrate layer," *Microw. Opt. Technol. Lett.*, vol. 52, no. 12, pp. 2812–2817, Dec. 2010.

[23] G. V. Trentini, "Partially reflecting sheet arrays," *IRE Trans. Antennas Propag.*, vol. 4, no. 4, pp. 666–671, Oct. 1956.

[24] J. Conrod, "Understanding when to use FR4 or high frequency laminates," Rogers Corp., Chandler, AZ, USA, Tech. Rep. 26-30, Sep. 2011.

[25] X. Zhang and L. Zhu, "Gain-enhanced patch antennas with loading of shorting pins," *IEEE Trans. Antennas Propag.*, vol. 64, no. 8, pp. 3310–3318, Aug. 2016.

[26] X. Zhang and L. Zhu, "High-gain circularly polarized microstrip patch antenna with loading of shorting pins," *IEEE Trans. Antennas Propag.*, vol. 64, no. 6, pp. 2172–2178, Jun. 2016.

[27] A. Foroozesh and L. Shafai, "Investigation into the effects of the patch-type FSS superstrate on the high-gain cavity resonance antenna design," *IEEE Trans. Antennas Propag.*, vol. 58, no. 2, pp. 258–270, Feb. 2010.

[28] N. Dang-Duy, N. Yoon, and C. Seo, "Gain enhancement of microstrip patch antenna with via holes structure," *IEICE Commun. Express*, vol. 8, no. 5, pp. 190–195, 2019.

[29] V. Palanisamy and R. Garg, "Rectangular ring and H-shaped microstrip antennas-alternatives to rectangular patch antenna," *Electron. Lett.*, vol. 21, no. 19, pp. 874–876, Sep. 1985.

[30] J. R. Aguilar, M. Beadle, P. T. Thompson, and M. W. Shelley, "The microwave and RF characteristics of FR4 substrates," in *Proc. IEE Colloq. Low Cost Antenna Technol.*, Feb. 1998, pp. 2/1–2/6.
[31] E. L. Holzman, "Wideband measurement of the dielectric constant of an FR4 substrate using a parallel-coupled microstrip resonator," *IEEE Trans. Microw. Theory Techn.*, vol. 54, no. 7, pp. 3127–3130, Jul. 2006.

DUY-NINH DANG received the B.S. degree from the School of Electronics and Telecommunications, Hanoi University of Science and Technology, Hanoi, Vietnam, in 2013. He is currently pursuing the Integrated master's and Ph.D. degree with the Department of Information Communication, Materials, and Chemistry Convergence Technology, Soongsil University, Seoul, South Korea.

His current research interests include high-gain antenna, power amplifiers, metamaterials, and wireless power transfer.

CHULHUN SEO (M'97–SM'14) received the B.S., M.S., and Ph.D. degrees from Seoul National University, Seoul, South Korea, in 1983, 1985, and 1993, respectively.

From 1993 to 1995, he was with the Massachusetts Institute of Technology (MIT), Cambridge, MA, USA, as a Technical Staff Member. From 1993 to 1997, he was with Soongsil University, Seoul, South Korea, as an Assistant Professor. From 1999 to 2001, he was a Visiting Professor with the MIT. From 1997 to 2004, he was an Associate Professor with Soongsil University. Since 2004, he has been a Professor of electronic engineering with Soongsil University. He was the Chairman of the IEEE MTT Korea Chapter, from 2011 to 2014. He is the President of the Korean Institute of Electromagnetic Engineering and Science (KIEES) and the Dean of Information and Telecommunications College, Soongsil University. He is the Director of the Wireless Power Transfer Research Center, supported by the Korean Government's Ministry of Trade, Industry and Energy, and the Metamaterials Research Center, supported by Basic Research Laboratories (BRL) through an NRF grant funded by the MSIP, and the Center for Intelligent Biomedical Wireless Power Transfer, supported by the National Research Foundation of Korea (NRF) funded by the MSIP. His research interests include wireless technologies, RF power amplifiers, and wireless power transfer using metamaterials.